Journal of Optics

Chirped photonic crystal for spatially filtered optical feedback to a broad-area laser

To cite this article before publication: Carsten Bree *et al* 2018 *J. Opt.* in press https://doi.org/10.1088/2040-8986/aada98

Chirped photonic crystal for spatially filtered optical feedback to a broad-area laser

C. Brée[1], D. Gailevičius[2], V. Purlys[2], G. G. Werner[3,4], K. Staliunas[3,5], A. Rathsfeld[1], G. Schmidt[1], M. Radziunas[1]

E-mail: Carsten.Bree@wias-berlin.de

[1] Weierstrass Institute, Mohrenstrasse 39, 10117 Berlin, Germany.

[2] Laser Research Center, Vilnius University, Sauletekio Ave. 10, 10222 Vilnius, Lithuania

[3] Departament de Fisica, Universitat Politècnica de Catalunya, 08222 Terrassa, Spain

[4] Monocrom S.L., C/Vilanoveta, 6, 08800 Vilanova i la Geltrú, Spain

[5] Institució Catalana de Recerca i Estudis Avançats, Passeig Lluis Companys 23, 08010 Barcelona, Spain

Abstract. We derive and analyze an efficient model for reinjection of spatially filtered optical feedback from an external resonator to a broad area, edge emitting semiconductor laser diode. Spatial filtering is achieved by a chirped photonic crystal, with variable periodicity along the optical axis and negligible resonant backscattering. The optimal chirp is obtained from a genetic algorithm, which yields solutions that are robust against perturbations. Exemplary numerical simulations of the composite system with our optoelectronic solver indicate that spatially filtered reinjection can enhance lower-order transversal optical modes in the laser diode and, consequently, improve the spatial beam quality.

1. Introduction

Semiconductor laser diodes (DLs) with optical feedback from an external cavity (EC) are experimentally and theoretically extensively studied dynamical systems showing a huge variety of different steady and dynamic states [1]. The majority of works on the ECDL systems is devoted to the study of the transversally-single mode narrow-waveguide DLs, for instance the pioneering work of Lang and Kobayashi [2] which has been referred to over 1000 times. In contrast to single lateral (transverse) mode lasers, a substantial width (x-coordinate) of the broad-area (BA) DLs leads to emission on multiple lateral optical modes, therefore the proper modeling of the spatiotemporal dynamics in these DLs should be performed by at least 1 (time) + 2 (space) - dimensional partial differential equations [3, 4]. Hence, the detailed experimental and theoretical study of BA-ECDLs and high-power (HP) BA-ECDLs, in particular, becomes much more complex [4, 5, 6, 7, 8, 9, 10, 11, 12, 13, 14, 15]. Due to potential applications of BA-HPDLs as high-power optical sources, the majority of works on BA-HPECDL systems are discussing methods for tailoring the emitted beam and improving the beam quality by optical feedback from a properly designed EC [8, 9, 10, 11, 12], study the damages implied by unwanted reinjection of the optical fields [13], or analyze the optical modes governed by the reduced-dimension PDE models [14, 15, 16]. In the present paper, we consider theoretical modelling and numerical studies of a BA-HPDL subjected to optical feedback from a particular type of EC, see Fig. 1(a), containing an anti-reflection (AR) coated photonic crystal (PhC) as spatial filtering element, see Fig. 1(b). An adequately chosen PhC translates specific angular components of the incident beam to corresponding larger diffraction order angles, see the schematic k_x-space representation of the incident and transmitted beams in panel (b). Such a diffracted forward propagating field misses the EC output coupler mirror and, therefore, is not reinjected into the BA-DL, which provides the spatial filtering functionality to the entire EC loop.

Variation of the longitudinal index modulation period g_z along the PhC provides broad flexibility in designing angular field transmission profiles, which we intend to exploit in the future for improving the quality of BA-HPDLs. The variety of the filtering profiles while featuring translational invariance in the transverse direction can be advantageos comparing to more restricted angular filtering used earlier in BA-HPECDLs [7, 9, 10, 17]. Our main task in this paper is to efficiently simulate the propagation of the optical field in the EC with an optimized PhC, and to properly calculate the field dynamics in the composite BA-ECDLs.

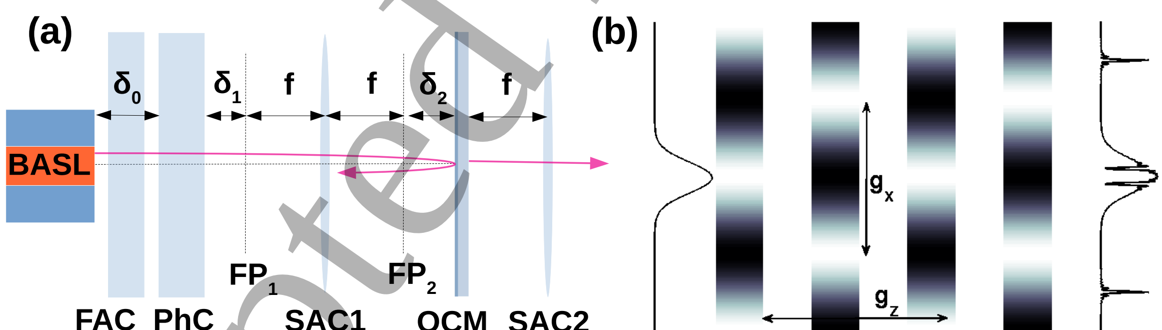

Figure 1: (a) Sketch of considered BA-ECDL setup: diode laser, fast axis collimator (FAC), PhC, slow axis collimating lenses (SAC), output coupler mirror (OCM). Dashed: front and rear SAC1 focal planes, with offsets δ_1 and δ_2 from PhC and OCM, respectively. δ_0: distance between DL and PhC. (b): scheme of a PhC with longitudinal and lateral periods g_z and g_x as well as k_x-space representation of the incident (left) and transmitted (right) beams.

2. Modeling of BA-DLs with optical feedback

To simulate the dynamics of BA-DLs we used the 2 (space) + 1 (time) dimensional traveling wave (TW) model [18] combined with the parallel solver BALaser [19], developed at the Weierstrass Institute in Berlin and used on the multicore compute servers there [20]. According to the TW model, the spatiotemporal evolution of the slowly varying complex amplitudes of two waves $E^+(z,x,t)$ and $E^-(z,x,t)$, counterpropagating along the longitudinal axis (z-coordinate), is governed by the following TW equations on the interval $z \in (-l, 0)$,

$$\frac{1}{v_g}\partial_t E^{\pm} = \left[\mp\partial_z - \frac{i}{2k_0\overline{n}}\partial_{xx} - i\beta\right] E^{\pm} + F_{sp}^{\pm}, \tag{1a}$$

$$E^+(-l,x,t) = \sqrt{R_r}E^-(-l,x,t), \tag{1b}$$

$$E^-(0,x,t) = \sqrt{R_f}E^+(0,x,t) + (1-R_f)[\mathcal{F}E^+](x,t). \tag{1c}$$

Here, v_g, $k_0 = 2\pi/\lambda_0$, $\overline{n}$, and $F_{sp}^{\pm}$ are the group velocity of light, the free-space central wavenumber for the operating wavelength $\lambda_0 = 975\,\mathrm{nm}$, the reference refractive index, and the Langevin noise term, respectively. The complex propagation factor $\beta(z,x,t)$ accounts for linear and nonlinear (two-photon) absorption [21], during the growth of the laser induced refractive index profile, as well as the gain and the refractive index change in the semiconductor material. The last two factors depend on the excess carrier density and take into account nonlinear gain compression [21], material gain dispersion [22], and the static refractive index change due to Joule heating [3]. The dynamics of the carrier densities is governed by the diffusive rate equation, where carrier diffusion and injected current (pump) at the active zone are determined by solving the carrier spreading problem in the lateral (x) and vertical (y) cross sections of the BA-DL device simultaneously [23]. The parameters R_r and R_f (which are 0.95 and 0.04 in the example considered below) are the field intensity reflection and transmission at the rear and front facets $z = -l$ and $z = 0$ of the diode (l: the length of the DL), *cf.* Refs. [21, 18] for more details on the model and typical diode parameters.

Assuming that the index guiding along the vertical axis of the DL as well as the beam collimation by the FAC are perfect, the vertical field distributions are eliminated, and the optical feedback $\mathcal{F}$ in Eq. (1c) is given in terms of a 1D- in space general linear integral operator,

$$[\mathcal{F}E^+](x,t) = \int_{-\infty}^{t}\int_{\mathbb{R}} K(x',t',x,t)E^+(0,x',t')dx'dt', \tag{2}$$

where the kernel function $K(x',t',x,t)$ depends on the configuration of the EC. For its construction, we exploit Huygens-Fresnel integrals within each optical element, see Fig. 1(a). For a perfect EC with vanishing offsets and no PhC [17], this procedure implies $K(x',t',x,t) = \eta\delta(x+x')\delta(t'-t+\tau)$, where δ is the Dirac delta function, τ is the field roundtrip time in the EC, and η accounts for the field reflectivity at the OCM and the constant phase shifts at the SAC lens.

For an extensive numerical calculation of the compound system, it is crucial to derive efficient approximations of the kernel function K in (2), and, particularly, kernels K_{PhC} and K'_{PhC}, which enter the definition of the overall kernel K and mimic the optical transmission through and the backscattering from the PhC according to

$$E_{\mathrm{transmitted}}(x,t) = \int_{-\infty}^{t} \int_{\mathbb{R}} K_{\mathrm{PhC}}(x',t',x,t) E_{\mathrm{incident}}(x',t') dx' dt',$$
$$E_{\mathrm{reflected}}(x,t) = \int_{-\infty}^{t} \int_{\mathbb{R}} K'_{\mathrm{PhC}}(x',t',x,t) E_{\mathrm{incident}}(x',t') dx' dt',$$

respectively. To describe the PhC part of the optical propagation within the EC, we investigate two different models. The first, and more complex, model relies on the solution of Maxwell's equations. The linear kernels K_{PhC} and K'_{PhC} are, in general, nonlocal in time and space. Our second model follows from a beam propagation method (BPM), which neglects backscattering ($K^r_{\mathrm{PhC}} = 0$) as well as angular dependencies of optical pathlengths. The resulting kernel K is local in time, which is beneficial for its implementation into our solver. A comparison of these two models reveals conditions under which the BPM provides a reasonable approximation. A previously reported good agreement of measurements and BPM-based simulations of the single pass transmission of the optical field through the optimized PhC [24] allows us to trust in the BPM. Since suitably manufactured PhCs bear a strong potential for tailoring the far-field characteristics of a transmitted beam [25], we focus on modelling and efficient implementation of the kernel function K and the resulting delay term (2) into our parallel solver [19].

3. Field propagation within the PhC

3.1. Rigorous coupled-wave analysis

For an accurate description of light propagation through a periodically modulated medium, one has to solve a boundary value problem for the time-harmonic Maxwell system and an incident plane wave of prescribed polarization, incident angle, and wavelength. While modeling, definition of appropriate radiation conditions, and solution theory is still open for the case of a PhC in a semi-infinite half-space (*cf.* a first approach in [26]), the case of a finite PhC layer is covered by the well-established theory and the numerics for electro-magnetic gratings. The complex valued reflection and transmission amplitudes R_j, T_j for each diffraction order j can be accessed. Here, we employ the method of rigorous coupled-wave analysis (RCWA). The time-harmonic Maxwell system is rewritten as an ordinary differential equation for the vector of z-dependent lateral Fourier coefficients of the transversal electro-magnetic field components. The underlying domain is split into several slices such that the refractive index is z-independent in each slice, and, for each slice, the differential equation can be solved by an eigenvalue decomposition. For PhCs with low contrast and smooth variation of $\bar{n}$ in the transversal x-direction, as considered in this work, *cf.* Fig. 1(b), the Fourier-mode expansion of the field can be truncated to a small number of modes with good accuracy, *cf.* [27, 28, 29].

For the simulation, we choose a PhC with background refractive index $\bar{n} = 1.5$ and lateral period $g_x = 2.4\mu$m. To justify the effect of spatial filtering by resonant scattering into higher diffraction orders, we performed calculations for different values of index modulation depth Δn_0. In Fig. 2(a), we show the obtained transmission efficiency

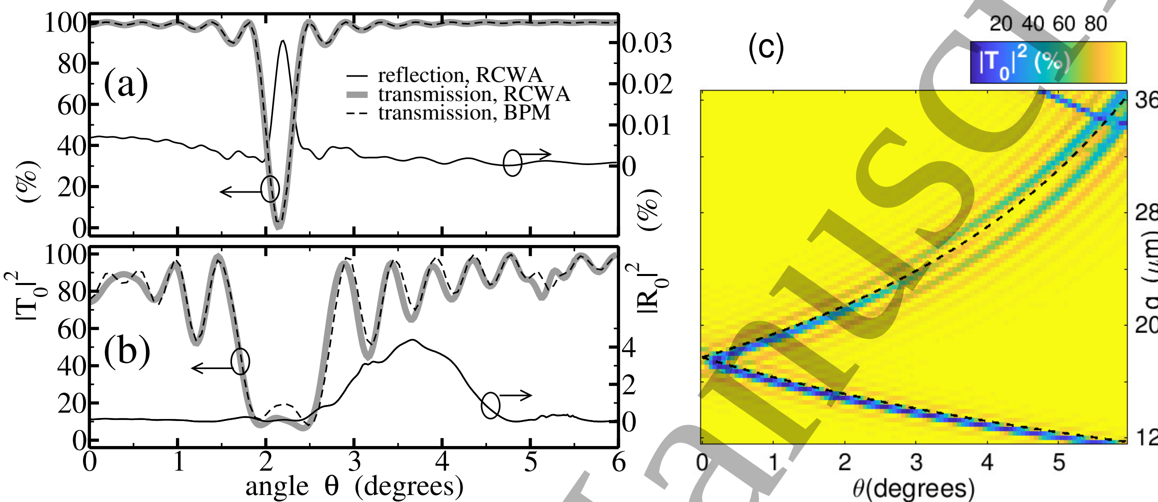

Figure 2: Parameter study for PhC with $g_x = 2.4\mu$m and 24 periods along z. (a): $|T_0|^2$ (thick gray) and $|R_0|^2$ (thin black), RCWA. Dashed: $|T_0|^2$, BPM. PhC parameters: $\Delta n_0 = 0.004$, $g_z = 21.4\mu$m (b): same, but $\Delta n_0 = 0.02$. (c): $|T_0|^2$ versus θ and g_z, $\Delta n_0 = 0.006$. Dashed: filtering angles vs. g_z, Eq. (3).

$|T_0|^2$, for a PhC with index modulation $\Delta n_0 = 0.004$ and 24 longitudinal periods with $g_z = 21.4\mu$m. In case of small incidence angles θ, resonant deflection of optical energy from the central lobe to the first diffraction orders occurs at

$$\sin\theta = \pm\frac{\lambda_0}{2g_x}|Q-1|, \tag{3}$$

whith a geometric resonance factor $Q = 2g_x^2\bar{n}/g_z\lambda_0$, *cf.* [30]. For the chosen PhC parameters, this resonance condition results in filtering angles at around 2°. The AR coatings suppress reflections from the PhC-air interfaces, which reveals only weak resonant backscattering $< 0.04\%$ from within the PhC, see thin black curve in Fig. 2(a). For increased index modulation of $\Delta n_0 = 0.02$, the transmission efficiency $|T_0|^2$ is shown in panel (b), with a considerably broader transmission gap around 2°. The corresponding backscattering efficiency $|R_0|^2$ shows a massive increase to about 4%, comparable to the reflectivity of the OCM. For suppressing divergent lateral modes with spatially filtered feedback, such a large amount of backscattering is unacceptable.

Finally, we calculated $|T_0|^2$ versus longitudinal period g_z in an angular range $|\theta| < 6°$, the typical beam divergence of semiconductor laser diodes, *cf.* Fig. 2(c). Again, we observe sharp transmission gaps at angles depending on g_z. In fact, closer inspection of Eq. (3) yields two branches for the filtering angle as a function of g_z. These are indicated by dashed lines for fixed wavelength λ_0, $g_x = 2.4\mu$m, and $\bar{n} = 1.5$.

A comparison with RCWA results shows that Eq. (3) accurately predicts the angular positions of the transmission gaps.

3.2. Beam propagation method and its numerical implementation

While the RCWA provides an accurate solution of the time-harmonic Maxwell equations, the computationally fast, but approximate BPM is more suitable for the optimization calculations. In paraxial approximation, it can be derived from the TW equation (1a) for the forward field component E^+, upon eliminating all nonlinear and dispersive contributions to the propagation constant and polarization density. Instead, only the contribution of refractive index modulation $\Delta n(x, z)$ is taken into account. As the PhC deflects radiation to large lateral angles, we increase the accuracy of our BPM by replacing the paraxial diffraction operator $\sim \partial_{xx}$ in Eq. (1a) by a pseudo-differential operator [31], which accurately accounts for the forward-branch $k_0 > 0$ of the spatial dispersion relation $k_x^2 + k_z^2 = k_0^2$. The resulting PDE, which is first-order with respect to z, is an envelope approximation of the second-order Helmholtz equation. For given initial condition $\hat{E}(k_x, z_0)$, the initial value problem has the general solution $\hat{E}(k_x, z) = \sum_{j=-J}^{J} T_j(k_x; z, z_0)\hat{E}(k_x + 2\pi j/g_x, z_0)$, with complex transmission amplitudes T_j for the j-th diffraction order. The introduced truncation threshold J accounts for the fact that the intensity scattered into higher-order sidebands ($J \gtrsim 2$) is neglegible for the considered weak index contrast PhCs. Therefore, the PhC propagator $\hat{K}_{\text{PhC}}$ has a sparse, $(2J + 1)-$banded matrix structure, where here and in the following, $\hat{}$ denotes k_x-space counterparts of linear integral operators. The complex amplitudes T_j can be obtained by semi-analytic integration of the envelope equation for suitable initial conditions, using an eigenvector decomposition technique [32]. With the obtained PhC propagator $\hat{K}_{\text{PhC}}$, we can proceed to build a matrix model for the overall EC kernel K, Eq. (2). First of all, the RCWA results indicate a negligible wavelength dependence of transmission and reflection efficiencies of the considered AR-coated PhCs in a spectral range around $\lambda_0 = 975\,\text{nm}$, with width of $\Delta\lambda \approx 5\,\text{nm}$ corresponding to the characteristic spectral bandwidth of the BA-DL emission, with the noted exception of PhCs exhibiting pronounced resonant backscattering. Since the latter are of little practical use for the current study, it is plausible to assume that the full kernel is local in time,

$$K(x', t', x, t) = \bar{K}(x', x)\delta(t' - t + \tau) \quad \Rightarrow \quad [\mathcal{F}E^+](x, t) = \int_{\mathbb{R}} \bar{K}(x', x)E^+(0, x', t - \tau)dx',$$

which tremendously simplifies the numerical implementation of the model and, in many cases, admits efficient methods for the estimation of the optical feedback term.

On the discrete numerical level, the last integral expression is equivalent to the matrix-vector product,

$$[\mathcal{F}E^+]_h(t) = \bar{\mathbf{K}}_h E_h^+(0, t - \tau),$$

where the subscript index $_h$ stands for discrete space in the lateral x-direction, the vector-functions $E_h^+(0, t - \tau)$ and $[\mathcal{F}E^+]_h(t)$ represent the (discretized) emitted and the reinjected fields at the front facet of the diode, whereas $\bar{\mathbf{K}}_h$ is a large $(N_x \times N_x)$-dimensional matrix (N_x: number of equidistant lateral discretization steps in the considered computational domain). The matrix $\bar{\mathbf{K}}_h$ can be further factorized as $\bar{\mathbf{K}}_h = \mathbf{K}_b\mathbf{K}_c\mathbf{K}_f$. Here, $\mathbf{K}_f$,$\mathbf{K}_b$ are forward resp. backward propagators given by

$$\mathbf{K}_f = \mathbf{K}_{\delta_1}\mathbf{K}_{\mathrm{PhC}}\mathbf{K}_{\delta_0}, \quad \mathbf{K}_b = \mathbf{K}_{\delta_0}\mathbf{K}_{\mathrm{PhC}}\mathbf{K}_{\delta_1}.$$

with a discrete x-space counterpart $\mathbf{K}_{\mathrm{PhC}}$ of the PhC propagator $\hat{K}_{\mathrm{PhC}}$ introduced above, and $\mathbf{K}_{\delta_0}, \mathbf{K}_{\delta_1}$ being the propagators through the laterally homogeneous media (FAC, air gaps), *cf.* Fig. 1(a). In k_x-space, $\hat{\mathbf{K}}_f, \hat{\mathbf{K}}_b$ have a sparse, band matrix structure inherited from $\hat{\mathbf{K}}_{\mathrm{PhC}}$, which is beneficial for numerical evaluation. The propagator $\mathbf{K}_c$ describes the field propagation from focal plane FP1 towards the OCM and back. In x-space, it is anti-diagonal and yields a mirror image of the complex optical field, multiplied, for non-vanishing offset δ_2, by a phase factor with parabolic dependence on x *cf.* [16]. For compactness of presentation, we introduce a matrix representation $\mathbf{D}$ of the discrete Fourier transform (DFT) which maps from x to k_x-space. With this, our numerical algorithm for the computation of the optical reinjection is given by

$$[\mathcal{F}E_h^+](0,t) = \left[\mathbf{D}^{-1}\hat{\mathbf{K}}_b\mathbf{D}\mathbf{K}_c\mathbf{D}^{-1}\hat{\mathbf{K}}_f\mathbf{D}\right]\mathbf{E}^+(0,t-\tau), \tag{4}$$

For simulating the optical field and carrier dynamics in the BA-DL subject to filtered reinjection, the factors $\mathbf{K}_c, \hat{\mathbf{K}}_b, \hat{\mathbf{K}}_f$ are initially precalculated and fed into our optoelectronic solver. With respect to numerical complexity of our modeling approach, we emphasize that the action of the DFT matrix $\mathbf{D}$ is calculated using the Cooley-Tukey fast Fourier transform (FFT) algorithm. In consequence, compared to the $\sim N_x^2$ operations required for the full matrix-vector multiplication, the described factorization of $\bar{\mathbf{K}}_h$ significantly reduces the numerical effort to a complexity of $\sim N_x \ln N_x$.

It remains to identify the limits of validity of the BPM used for modeling the PhC propagators contained in K. For each of the PhC structures in Fig. 2, we calculate the corresponding transmission efficiencies. As shown by the black curve in Fig. 2(a), we observe excellent agreement for low index contrast $\Delta n_0 = 0.004$, and slightly larger deviations for $\Delta n_0 = 0.02$, *cf.* Fig. 2(b), which is prohibitive due to large resonant backscattering. Altogether, extensive simulations with the RCWA solver reveal that the BPM yields reasonable results for lateral periods $g_x \gtrsim 2\mu\mathrm{m}$ (i.e., larger than approximately twice the wavelength), longitudinal periods g_z corresponding to $Q \in [0.4, 1.6]$, refractive index contrast of the order of $\Delta n \sim 0.01$, and not more than a few tens of longitudinal periods. In that case, the RCWA also predicts a tolerable intensity in the backscattered field below the 1%-level.

4. Tailoring chirped PhC

The above considerations indicate that broader angular transmission gaps, which are potentially useful for spatial filtering, are obtained either for larger index contrast or increased number of longitudinal layers. However, in case of strictly periodic PhCs, this comes at the cost of increased resonant backscattering. In the following, we show that PhCs with variable longitudinal periods avoid this detrimental side effect. The use and versatility of longitudinally chirped PhCs for spatial filtering of laser beams have first been discussed in [32, 33]. Here, we solve the inverse problem of finding an optimized longitudinal chirp for a prescribed transmission efficiency $|T_0|^2$ with broad angular gaps. In the examples considered below in this paper we seek to fit the transmission efficiency $|T_0|^2$ to the selected target function $\mathcal{T}$ which is 0.2 between $2°$ and $4°$ but unity outside of this interval. The total angular range of the considered example is $[0°, 6°]$, whereas the transmission profile for the negative angles is symmetric with respect to the zero angle. The choice of this filtering profile was motivated by the around six degree-broad divergence of the experimentally available BA-HPDL emission as well as by the technological restrictions fabricating longer multi-layer chirped PhCs.

Using a suitable nonlinear optimization routine, we maximize a fitness functional $F : \vec{d}_z \in \mathbb{R}^N \to \mathbb{R}^+$, *cf.* [31]. Here, the N components d_z^j of $\vec{d}_z$ correspond to longitudinal layer thicknesses, where each layer consists of two slices of thickness $d_z^j/2$, namely, a slice with harmonic lateral index modulation $\bar{n}+\Delta n$ and a homogeneous slice with refractive index $\bar{n}$. Between adjacent layers, there is a π-phaseshift in the modulated slice.

The fitness functional favors vectors $\vec{d}_z$ leading to chirped PhCs with admissible transmission efficiency $|T_0|^2$. For the current study, we used a fixed refractive index modulation depth of $\Delta n_0 = 0.012$ and $N = 48$ longitudinal layers. For optimization, we use a genetic algorithm which prevents convergence to a narrow local minimum and favors robust solutions [34]. Each iteration step of the genetic algorithm requires calculations of $|T_0|^2$ and $F[\vec{d}_z]$ for all members $\vec{d}_z$ of the genetic pool. For this, we employ the numerically more efficient BPM and compare the final optimization result with the RCWA. In Fig. 3, we present an optimization result obtained for the considered target function $\mathcal{T}$. The optimized chirp vector $\vec{d}_z^{\mathrm{opt.}}$ is shown in panel (a), and the resulting transmission efficiency is depicted by the dashed curve in panel (b), with broad transmission gap between $2°$ and $4°$. The thick gray line in panel (b) corresponds to the transmission amplitude obtained by feeding $\vec{d}_z^{\mathrm{opt.}}$ into the RCWA solver. It exhibits reasonable agreement with the BPM results. Furthermore, the corresponding reflection efficiency does not exceed 0.13% in the considered angular range, *cf.* panel (b). Finally, robustness of the optimized solution versus perturbations is established numerically. Forty displacement vectors $\vec{\xi}_\delta \in \mathbb{R}^N$ are drawn randomly, with components uniformly distributed in $[-\delta, \delta]$, and added to $\vec{d}_z^{\mathrm{opt.}}$. Transmission efficiencies, averaged over the realizations of $\vec{\xi}_\delta$, are depicted in panels (c) (BPM) and (d) (RCWA), for $\delta = 10\,\mathrm{nm}$, $\delta = 100\,\mathrm{nm}$ and $\delta = 1000\,\mathrm{nm}$. We find remarkable robustness, with a noise tolerance well within the current accuracy limits of direct femtosecond laser writing [31].

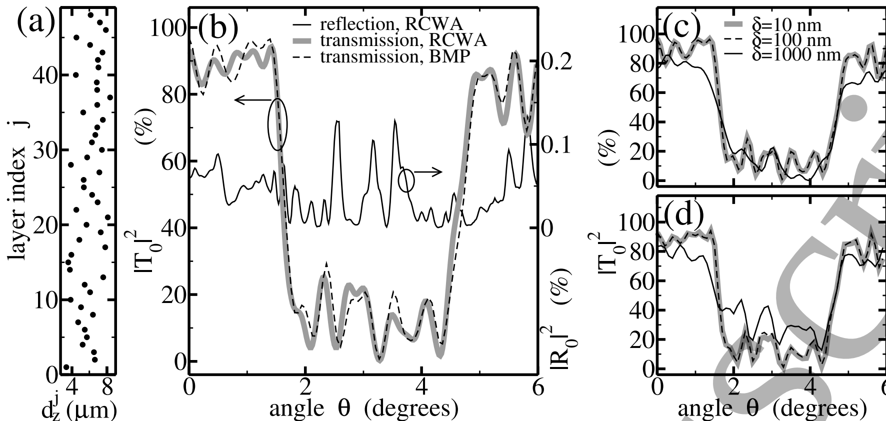

Figure 3: (a): optimized chirp $\vec{d}_z^{\,\text{opt.}}$. (b): corresponding transmission efficiency $|T_0|^2$. Thick gray: RCWA, thin dashed: BPM, thin solid: $|R_0|^2$. (c): $|T_0|^2$ for perturbed chirp $\vec{d}_z^{\,\text{opt.}} + \vec{\xi}_\delta$ (BPM), $\delta = 10$, 100, and 1000 nm (gray, dashed, solid black). (d): same as (c), RCWA

5. Example: shaping of the BA-DL emission by filtered optical feedback

The above derived BPM-based model for the field propagation within the EC containing the PhC was implemented into our software kit BALaser [19] used for simulation of dynamics in BA-HPDLs. To test whether the suggested EC configuration can be employed to the shaping of the laser emission, we simulated a 1 mm-long and 100 μm-broad BA-HPDL with and without the feedback from the EC containing the optimized PhC filter, see Fig. 4. The bias current of this laser was 2.8 A. In absence of the EC, it emits a high-power $P_0 = 2.82$ W beam with divergence angle $\theta_{95} \sim 6^\circ$ and near field width $w_{95} = 92\mu$m, both evaluated at 95% power content. The lateral beam parameter product (BPP) and beam quality factor amount to $\text{BPP}_0 \sim 2.25\,\text{mm}\times\text{mrad}$ and $M_0^2 = \text{BPP}_0 \times \pi/\lambda \sim 7.3$, respectively. The brightness is $B_0 = P_0^2/M_0^2\lambda^2 \approx 0.4\,\text{W/sr}\cdot\mu\text{m}^2$, where it was assumed that the beam is diffraction limited in the vertical direction.

Next, we have simulated BA-DL with the EC containing the optimized PhC. Substituting the PhC with a homogeneous antireflection-coated glass block of the same dimensions and background refractive index, 1 : 1 imaging of the mirrored field configuration would be obtained for a perfectly aligned EC with vanishing EC offsets δ_2 and Δ_1, where

$$\Delta_1 := \delta_0 - l_{\text{FAC}}(1 - 1/\bar{n}_{\text{FAC}}) + l_{\text{PhC}}/\bar{n}_{\text{PhC}} + \delta_1.$$

The total width and the background refractive index of the considered PhC and FAC were $l_{PhC} = 0.289$ mm, $\bar{n}_{PhC} = 1.5$, and $l_{FAC} = 1.5$ mm, $\bar{n}_{FAC} = 1.5$, respectively, whereas the focal length of the SAC lenses was $f = 24$ mm. We performed simulations for $\delta_2 = 0$ and different values of the offset Δ_1. Optimal beam quality w.r.t. beam parameter product and beam brightness was achieved for $\Delta_1 \approx 1.5$ mm, *cf.* Fig. 4(a). Due to the radiation loss to the sidebands, see insert, a significant power fraction is lost from the central lobe, i.e., it contains only 78% of the total emitted power $P_{\text{tot.}} = 2.6$ W.

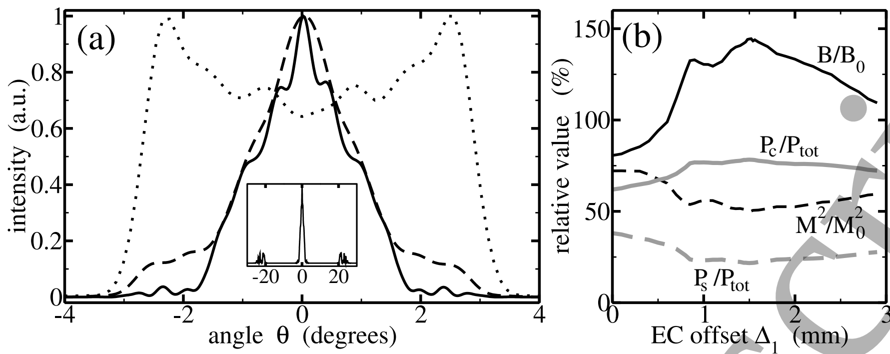

Figure 4: (a): BA-DL emission for $\Delta_1 = 1.5\,\mathrm{mm}$. Dashed: time-averaged Fourier transformed near field at BA-DL output facet. Solid: far field coupled out from EC. Dotted: BA-DL emission w/o EC. Insert: same, on larger angular scale. (b) brightness B (black solid), M^2 (black dashed) relative to case w/o EC. Gray, solid resp. dashed: power fractions $P_c/P_{\mathrm{tot.}}$, $P_s/P_{\mathrm{tot.}}$ in central- and sidelobes.

Nevertheless, as a main achievement of our theoretical study, we find that the spatially filtered optical feedback causes a significant improvement of the laser beam quality. In Fig. 4(b), we show the relative changes of brightness and beam quality factor M^2 compared to the corresponding factors B_0 and M_0^2 without reinjection. At optimum, the simulations show that brightness increases by 45%, while M^2 decreases by 50%. It is noteworthy that a significant shaping of the angular beam profile can be observed not only after its pass through the PhC but also directly after its emission from the diode, see dashed and solid black curves in Fig. 4(a). This observation confirms the suppression of the higher-order lateral optical modes of the BA-HPDL by an adequately designed spatially filtered optical feedback. Broader study and optimization simulations of BA-HPECDL devices are, however, out of the scope of the present paper.

6. Conclusions

In conclusion, we have performed efficient modeling and optimization of the beam propagation in the EC containing a PhC spatial filtering element. We have shown that, provided the refractive index contrast in the PhC is not exceeding the order of 10^{-2}, the backscattered intensity can be kept below 1% and the BPM can produce reliable field transmissions through the PhC. Our optimization of the PhC was aiming to reduce the radiation at $\pm[2^\circ, 4^\circ]$ angles to the optical axis during the single-pass of the beam through the PhC. The consequent exemplary simulations of the BA-HPECDL with this optimized PhC within the EC have demonstrated the suppression of the higher-order lateral optical modes of the BA-HPDL A more detailed theoretical and experimental study of the impact of filtered feedback to the beam quality of BA-HPDLs is in preparation and will be considered in our following paper.

Acknowledgments

This work was supported by the EUROSTARS Project E!10524 HIP-Lasers, as well as by Spanish Ministerio de Ciencia e Innovación, and European Union FEDER through project FIS2015-65998-C2-1-P. D.G. and V.P. acknowledge the financial support from "FOKRILAS" (Project No. P-MIP-17-190) from Research Council of Lithuania. We also acknowledge fruitful discussions with A. Lamacz, S. Reichelt, B. Schweizer, and H.-J. Wünsche.

References

[1] Kane D and Shore A (eds) 2005 *Unlocking Dynamical Diversity: Optical Feedback Effects on Semiconductor Lasers* (John Wiley & Sons)
[2] Lang R and Kobayashi K 1980 *IEEE J. of Quantum Electron.* **16** 347–355
[3] Wenzel H 2013 *IEEE J. Sel. Top. Quantum Electron.* **19** 1–13
[4] Simmendinger C, Preier D and Hess O 1999 *Opt. Express* **5** 48–54
[5] Lim J, Sujecki S, Lang L, Zhang Z, Paboeuf D, Pauliat G, Lucas-Leclin G, Georges P, MacKenzie R, Bream P, Bull S, Hasler K H, Sumpf B, Wenzel H, Erbert G, Thestrup B, Petersen P, Michel N, Krakowski M and Larkins E 2009 *IEEE J. Sel. Top. Quantum Electron.* **15** 993–1008
[6] Mandre S, Fischer I and Elsäßer W 2005 *Optics Communications* **244** 355–365
[7] Wolff S, Rodionov A, Sherstobitov V and Fouckhardt H 2003 *IEEE J. Quantum Electron.* 448–458
[8] Gaciu N, Gehrig E and Hess O 2008 Control of broad-area laser dynamics with delayed optical feedback *Handbook of Chaos Control* ed Schöll E and Schuster H G (Wiley VCH Verlag GmbH & Co. KGaA) pp 427–453
[9] Raab V and Menzel R 2002 *Opt. Letters* **27** 167–169
[10] Jechow A, Lichtner M, Menzel R, Radziunas M, Skoczowsky D and Vladimirov A 2009 *Optics Express* **17** 19599–19604
[11] Zink C, Niebuhr M, Jechow A, Heuer A and Menzel R 2014 *Optics Express* **22** 14108–14113
[12] Fouckhardt H, Kleinschmidt A K, Strassner J and Doering C 2017 *Advances in OptoElectronics* **2017** 5283850
[13] Hempel M, Chi M, Petersen P, Zeimer U and Tomm J 2013 *Appl. Phys. Lett.* **102** 023502
[14] Marciante J and Agrawal G 1996 *IEEE J. Quantum Electron.* **32** 1630–1635
[15] Takeda A, Shogenji R and Ohtsubo J 2013 *Optical Review* **20** 308–313
[16] Champagne Y, Mailhot S and McCarthy N 1995 *IEEE J. Quantum Electron.* **31** 795–810
[17] Wolff S, Messerschmidt D and Fouckhardt H 1999 *Opt. Express* **5** 32–37
[18] Spreemann M, Lichtner M, Radziunas M, Bandelow U and Wenzel H 2009 *IEEE J. of Quantum Electron.* **45** 609–616
[19] BALaser: a software tool for simulation of dynamics in Broad Area semiconductor Lasers. URL `http://www.wias-berlin.de/software/balaser`
[20] Radziunas M 2018 *The Int. J. of High Perform. Comp. Appl.* **32** 512–522
[21] Zeghuzi A, Radziunas M, Klehr A, Wünsche H J, Wenzel H and Knigge A 2018 *Opt. and Quantum Electron.* **50** 88
[22] Bandelow U, Radziunas M, Sieber J and Wolfrum M 2001 *IEEE J. of Quantum Electron.* **37** 183–188
[23] Radziunas M, Zeghuzi A, Fuhrmann J, Koprucki T, Wünsche H J, Wenzel H and Bandelow U 2017 *Optical and Quantum Electronics* **49** 332
[24] Gailevicius D, Koliadenko V, Purlys V, Peckus M, Taranenko V and Staliunas K 2016 *Sci. Rep.* **6** 34173
[25] Maigyte L and Staliunas K 2015 *Appl. Phys. Rev.* **2** 011102
[26] Lamacz A and Schweizer B 2016 *arXiv:1509.00683v2 [math.AP]*

[27] Popov E 2014 Chapter 7: Differential theory of periodic structures *Gratings: Theory and Numerical Applications* ed Popov E (Aix Marseille Université, Institut Fresnel UMR 7249: Presses Universitaires de Provence) chap 7

[28] Moharam M G and Gaylord T K 1981 *J. Opt. Soc. Amer.* **71** 811–818

[29] Nevière M and Popov E 2003 *Light propagation in periodic media* (New York, Basel: Marcel Dekker, Inc.)

[30] Radziunas M, Herrero R, Botey M and Staliunas K 2015 *J. Opt. Soc. Am. B* **32** 993–1000

[31] Gailevičius D, Purlys V, Peckus M, Gadonas R and Staliunas K 2017 *Annalen der Physik* **529** 1700165 ISSN 1521-3889 1700165 URL `http://dx.doi.org/10.1002/andp.201700165`

[32] Staliunas K and Sánchez-Morcillo V J 2009 *Phys. Rev. A* **79** 053807

[33] Purlys V, Maigyte L, Gailevičius D, Peckus M, Malinauskas M and Staliunas K 2013 *Phys. Rev. A* **87** 033805

[34] Fogel D B 2006 *Evolutionary Computation: Toward a New Philosophy of Machine Intelligence* 3rd ed (New York, Basel: Wiley-IEEE Press)